

# 1 Capsule Networks as Recurrent Models of

## 2 Grouping and Segmentation

3 Adrien Doerig<sup>a,†,\*</sup>, Lynn Schmittwilken<sup>a,†</sup>, Bilge Sayim<sup>b,c</sup>, Mauro Manassi<sup>d</sup> & Michael H. Herzog<sup>a</sup>

4 <sup>a</sup> Laboratory of Psychophysics, Brain Mind Institute, EPFL, Lausanne, 1015, Switzerland

5 <sup>b</sup> Institute of Psychology, University of Bern, 3012 Bern, Switzerland

6 <sup>c</sup> Univ. Lille, CNRS, UMR 9193- SCALab- Sciences Cognitives et Sciences Affectives, F-59000 Lille, France

7 <sup>d</sup> Department of Psychology, University of Aberdeen, Aberdeen, Scotland, UK

8 <sup>†</sup> Equal contributions

9 \* Corresponding author: adrien.doerig@gmail.com

10 Keywords: Vision, Neural Networks, Capsule Networks, Crowding, Global Shape Processing, Recurrent  
11 Processing

### 12 Abstract

13 Classically, visual processing is described as a cascade of local feedforward computations. Feedforward  
14 Convolutional Neural Networks (ffCNNs) have shown how powerful such models can be. Previously,  
15 using visual crowding as a well-controlled challenge, we showed that no classic model of vision,  
16 including ffCNNs, can explain human global shape processing (1). Here, we show that Capsule Neural  
17 Networks (CapsNets; 2), combining ffCNNs with a grouping and segmentation mechanism, solve this  
18 challenge. We also show that ffCNNs and standard recurrent networks do not, suggesting that the  
19 grouping and segmentation capabilities of CapsNets are crucial. Furthermore, we provide  
20 psychophysical evidence that grouping and segmentation is implemented recurrently in humans, and  
21 show that CapsNets reproduce these results well. We discuss why recurrence seems needed to  
22 implement grouping and segmentation efficiently. Together, we provide mutually reinforcing  
23 psychophysical and computational evidence that a recurrent grouping and segmentation process is  
24 essential to understand the visual system and create better models that harness global shape  
25 computations.

26

## 27 Author Summary

28 Feedforward Convolutional Neural Networks (ffCNNs) have revolutionized computer vision and are  
29 deeply transforming neuroscience. However, ffCNNs only roughly mimic human vision. There is a  
30 rapidly expanding literature investigating differences between humans and ffCNNs. Several findings  
31 suggest that, unlike humans, ffCNNs rely mostly on local visual features. Furthermore, ffCNNs lack  
32 recurrent connections, which abound in the brain. Here, we use visual crowding, a well-known  
33 psychophysical phenomenon, to investigate recurrent computations in global shape processing.  
34 Previously, we showed that no model based on the classic feedforward framework of vision, including  
35 ffCNNs, can explain global effects in crowding. Here, we show that Capsule Networks (CapsNets),  
36 combining ffCNNs with recurrent grouping and segmentation, solve this challenge. Lateral and top-  
37 down recurrent connections do not, suggesting that grouping and segmentation are crucial for  
38 human-like global computations. Based on these results, we hypothesize that one computational  
39 function of recurrence is to efficiently implement grouping and segmentation. We provide  
40 psychophysical evidence that, indeed, recurrent processes implement grouping and segmentation in  
41 humans. CapsNets reproduce these results too. Together, we provide mutually reinforcing  
42 computational and psychophysical evidence that a recurrent grouping and segmentation process is  
43 essential to understand the visual system and create better models that harness global shape  
44 computations.

## 45 Introduction

46 The visual system is often seen as a hierarchy of local feedforward computations (3), going back to  
47 the seminal work of Hubel and Wiesel (4). Low-level neurons detect basic features, such as edges.  
48 Higher-level neurons pool the outputs from the lower-level neurons to detect higher-level features  
49 such as corners, shapes, and ultimately objects. Feedforward Convolutional Neural Networks (ffCNNs)  
50 embody this classic framework of vision and have shown how powerful it can be (e.g., 5–8). However,  
51 despite their amazing success, ffCNNs only roughly mimic human vision. For example, they lack the  
52 abundant recurrent processing of humans (9, 10), perform differently than humans in crucial  
53 psychophysical tasks (1, 11), and can be easily misled (12–14). An important point of discussion  
54 concerns global visual processing. It was suggested that ffCNNs may focus mainly on local, texture-  
55 like features, while humans harness global shape level computations (1, 14–18; but see 19). For  
56 example, it was shown that changing local features, such as the texture or the edges of an object, can

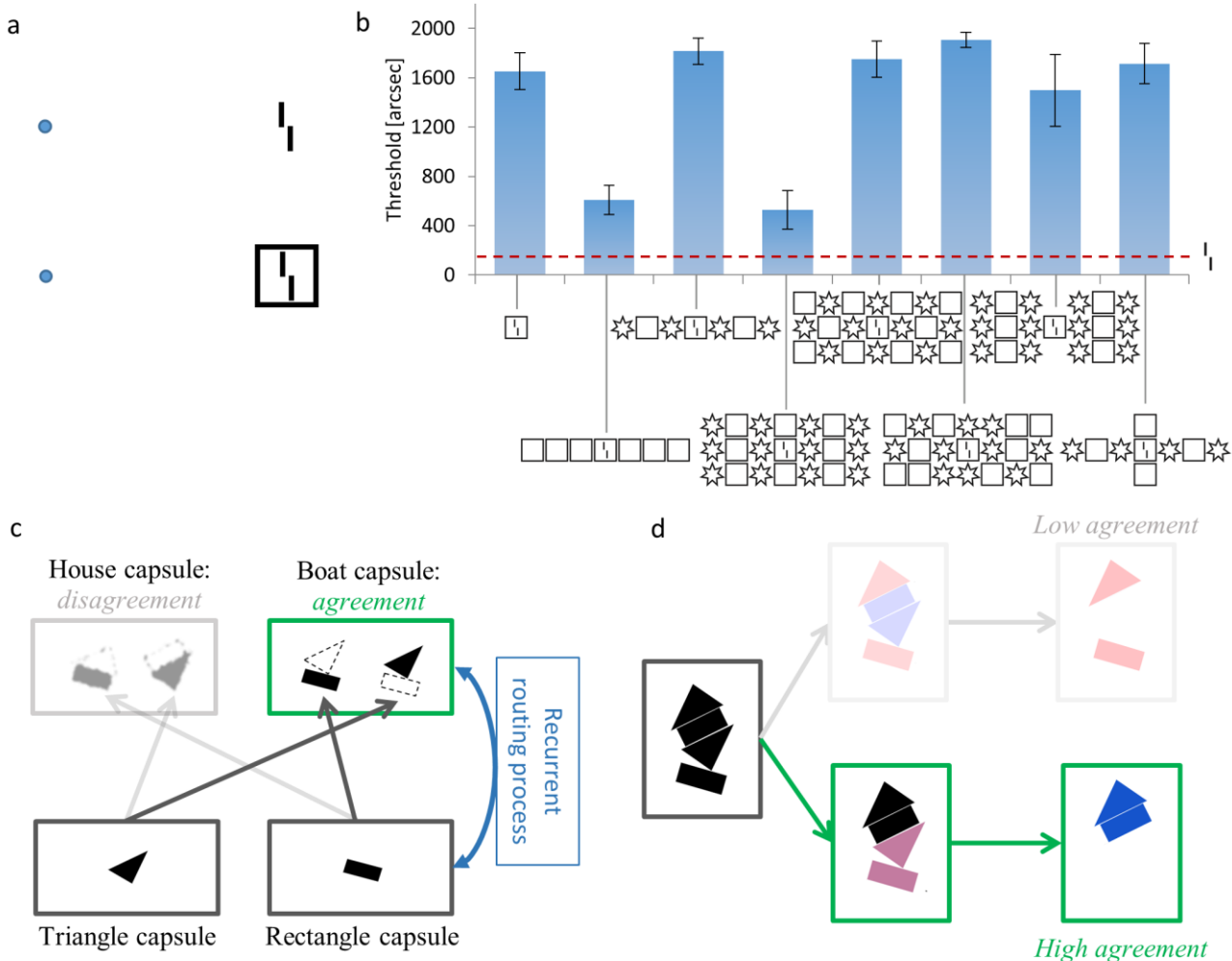
57 lead ffCNNs to misclassify it (14, 15). Humans, in contrast, can still easily classify the object based on  
58 its global shape.

59 There are no widely accepted diagnostic tools to specifically characterize global computations in  
60 neural networks. Models are usually compared either on computer vision benchmarks, such as  
61 ImageNet (20) or with neural responses in the visual system (21, 22). One drawback with these  
62 approaches is that the datasets are hard to control. Psychophysical results can be used to fill this gap  
63 and create well-controlled challenges for visual models, tailored to target specific aspects of vision  
64 (23). Here, we use visual crowding to specifically target global shape computations in humans and  
65 machines.

66 In crowding, objects that are easy to identify in isolation appear as jumbled and indistinct when clutter  
67 is added (1, 24–29). For example, a vernier target is presented, i.e., two vertical lines separated by a  
68 horizontal offset (Figure 1a). When the vernier is presented alone, observers easily discriminate the  
69 offset direction. When a flanking square surrounds the target, performance drops, i.e., there is strong  
70 crowding (30, 31). Surprisingly, *adding* more flanking squares *reduces* crowding strongly, depending  
71 on the configuration (Figure 1b; 29). Hence, the *global* configuration of visual elements across large  
72 regions of the visual field influences perception of the small vernier target. This global *uncrowding*  
73 effect occurs for a wide range of stimuli in vision, including foveal and peripheral vision, audition, and  
74 haptics (32–38). The ubiquity of (un)crowding in perception is not surprising since elements are rarely  
75 seen in isolation. Hence, any perceptual system needs to cope with crowding, i.e., isolating important  
76 information from clutter.

77 We have shown previously that these global effects of crowding *cannot* be explained by models based  
78 on the classic framework of vision, including ffCNNs (1, 18, 39). Here, we propose a new framework  
79 to understand these global computations. We show that Capsule Neural Networks (CapsNets; 2),  
80 augmenting ffCNNs with a recurrent grouping and segmentation process, can explain these complex  
81 global (un)crowding results in a natural manner. Two processing regimes can occur in CapsNets: a fast  
82 feedforward pass able to quickly process information, and a time-consuming recurrent regime to  
83 compute in-depth global grouping and segmentation. We will show that the human visual system  
84 indeed harnesses recurrent processing for efficient grouping and segmentation, and that CapsNets  
85 naturally explain these results. Together, our results suggest that a time-consuming recurrent  
86 grouping and segmentation process is crucial for global shape-level computations in both humans  
87 and artificial neural networks.

88



89

90 **Figure 1: a. Crowding:** Perception of visual elements deteriorates in clutter, an effect called crowding. In this example, a  
91 vernier (two vertical bars with a horizontal offset) becomes harder to perceive when a square flanker is added (fixate on  
92 the blue dots). **b. Uncrowding:** A vernier is presented in the visual periphery. The offset direction is easily reported (dashed  
93 red line; the y-axis shows the threshold, i.e., the minimal offset size at which observers can report the offset direction with  
94 75% accuracy). When a square flanker surrounds the vernier, performance deteriorates- a classic crowding effect. When  
95 more squares are added, performance recovers (uncrowding). Critically, the uncrowding effect depends on the global  
96 stimulus configuration. For example, if some squares are replaced by stars, performance deteriorates again (3<sup>rd</sup> bar; 25).  
97 **c. Routing by agreement in CapsNets:** Information propagates between layers of capsules through a recurrent routing  
98 process aiming to maximize agreement between capsules. Each capsule is a group of neurons whose activity vector  
99 represents the pose (such as position, orientation, etc.) of the feature it detects. In this toy example, lower-level capsules  
100 detect simple shapes such as triangles and rectangles. In the next layer, capsules have learnt combinations of these shapes.  
101 Here, the triangle capsule detects a tilted triangle and the rectangle capsule detects a tilted rectangle. Each of these  
102 capsules predicts what is represented at the next layer. For example, the triangle capsule predicts an upside-down house  
103 or a tilted boat, while the rectangle capsule predicts a tilted house or a tilted boat. The recurrent routing by agreement  
104 process routes information between the layers so that agreement is maximized. In this case, capsules agree about the  
105 tilted boat, but disagree about the house orientation. Hence, the routing by agreement suppresses activity in the house  
106 capsule and boosts activity in the boat capsule. **d. Grouping and segmentation in CapsNets:** This recurrent routing by

107 agreement process endows CapsNets with natural grouping and segmentation capabilities. Here, an ambiguous stimulus,  
108 which can be seen either as an upside-down house (top) or a house on a boat (bottom), is presented. The upside-down  
109 house interpretation leaves parts of the image unexplained and this causes disagreement. Hence, the routing by  
110 agreement will select the latter interpretations because it is the best explanation of the input and therefore maximizes  
111 agreement. Thereby, the house and boat are each grouped as an object and segmented into the corresponding higher-  
112 level capsules.

113

## 114 Results

### 115 Experiment 1: Crowding and Uncrowding Naturally Occur in CapsNets

116 In CapsNets, early convolutional layers extract basic visual features. Recurrent processing combines  
117 these features into groups and segments objects by a process called *routing by agreement*<sup>1</sup>. The en-  
118 tire network is trained end-to-end through backpropagation. *Capsules* are groups of neurons repre-  
119 senting visual features and are crucial for the routing by agreement process. Low-level capsules iter-  
120 atively predict the activity of high-level capsules in a recurrent loop. If the predictions agree, the cor-  
121 responding high-level capsule is activated. For example, if a capsule responds to a triangle above a  
122 rectangle detected by another capsule, they agree that the higher-level object should be a house and,  
123 therefore, the corresponding high-level capsule is activated (Figure 1c). This process allows CapsNets  
124 to group and segment objects (Figure 1d).

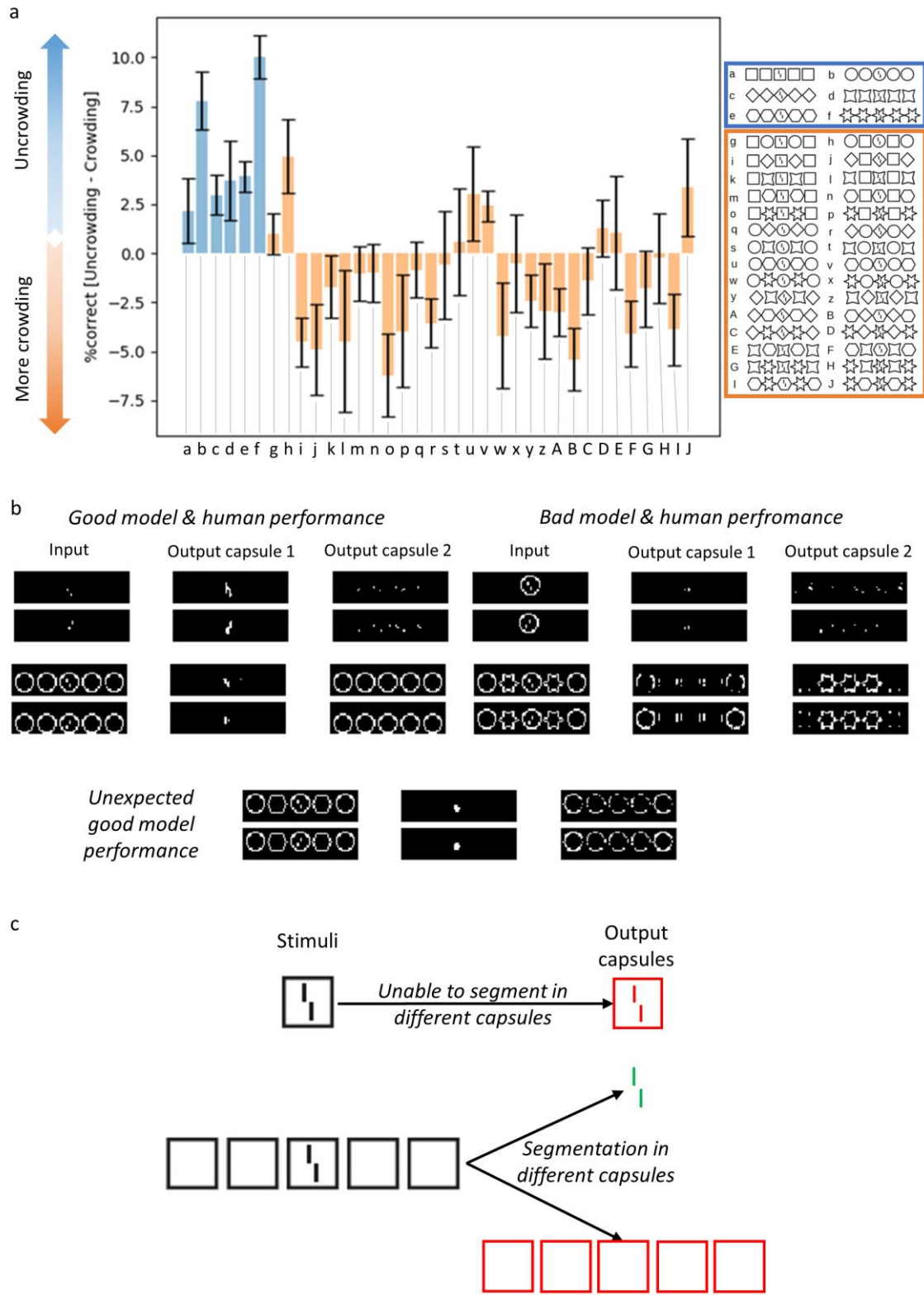
125 We trained CapsNets with two convolutional layers followed by two capsule layers to recognize  
126 greyscale images of vernier targets and groups of identical shapes (see Methods). During training,  
127 either a vernier or a group of identical shapes was presented. The network had to simultaneously  
128 classify the shape type, the number of shapes in the group, and the vernier offset direction.  
129 Importantly, verniers and shapes were never presented together during training, i.e., there were no  
130 (un)crowding stimuli during training.

131 When combining verniers and shapes after training, both crowding and uncrowding occurred (Figure  
132 2a): presenting the vernier target within a single flanker deteriorated vernier offset discrimination  
133 (crowding), and adding more identical flankers recovered performance (uncrowding). Adding config-  
134 urations of alternating different flankers did not recover the network's performance, similarly to hu-  
135 man vision. Small changes in the network hyperparameters, loss terms or stimulus characteristics do  
136 not affect these results (supplementary material). As a control condition, we checked that when the

---

<sup>1</sup> In most implementations of CapsNets, including ours and (2), the iterative routing by agreement process is not explicitly implemented as a “standard” recurrent neural network processing sequences of inputs online. Instead, there is an iterative algorithmic loop (see (2) for the algorithm), which is equivalent to recurrent processing.

137 vernier target is presented outside the flanker configuration, rather than inside, there was no perfor-  
138 mance drop (supplementary material). Hence, the performance drop in crowded conditions was not  
139 merely to the simultaneous presence of the target and flanking shape in the stimulus.  
140 Reconstructing the input image based on the network's output (see Methods) shows that (un)crowd-  
141 ing occurs through grouping and segmentation (figure 2b). Crowding occurs when the target and  
142 flankers cannot be segmented and are therefore routed to the same capsule. In this case, they inter-  
143 fere because a single capsule cannot represent well two objects simultaneously due to limited neural  
144 resources. This mechanism is similar to pooling: information about the target is pooled with infor-  
145 mation about the flankers, leading to poorer representations. However, if the flankers are segmented  
146 away and represented in a different capsule, the target is released from the flankers' deleterious ef-  
147 fects and *uncrowding* occurs (Figure 2c). This segmentation can only happen if the network has learnt  
148 to group the flankers into a single higher-level object represented in a different capsule than the ver-  
149 nier target. Segmentation is facilitated when more flankers are added because more low-level cap-  
150 sules agree about the presence of the flanker group.  
151 Alternating configurations of different flankers, as in the third configuration of Figure 1b, usually do  
152 not lead to uncrowding (29). In some rare cases, the network produced uncrowding with such config-  
153 urations (stimuli h, u, v & J; Figure 2). Reconstructions show that in these cases the network simply  
154 could not differentiate between different shapes of the flankers (e.g. between circles and hexagons),  
155 which therefore formed a group for the network and were segmented away from the target (Figure  
156 2b). This further reinforces the notion that grouping and segmentation differentiate crowding from  
157 uncrowding: whenever the network reaches the conclusion that flankers form a group, segmentation  
158 is facilitated. When this happens, the vernier and flankers are represented in different capsules, lead-  
159 ing to good performance.  
160



161

162 **Figure 2: a. CapsNets explain both crowding and uncrowding:** The x-axis shows the various stimuli. We used 6 different  
 163 flanker shape types and tested all configurations with 5 identical or alternating shapes (e.g., 5 squares, 5 circles, circle-  
 164 square-circle-square-circle, etc; see Methods). Performance is shown on the y-axis as the % correct for each stimulus  
 165 minus the % correct with only the central single flanker. For example, in column *a*, vernier offset direction is easier to read  
 166 out with 5 square flankers than with 1 square flanker, as expected. Error bars are the standard error over 10 network  
 167 trainings (we used 10 networks to match the typical number of observers in human experiments; 29, 40). The blue bars

168 represent configurations for which *uncrowding* is expected (blue bars larger than 0.0 are in accordance with the human  
169 data) and orange bars represent configurations for which *crowding* is expected (orange bars smaller than or around 0.0  
170 are in accordance with the human data). **b. Reconstructions:** We reconstructed the input image based on the output  
171 capsules' activities (see Methods). The reconstructions based on the two most activated capsules are shown. When the  
172 vernier is presented alone (top left), the reconstructions are good. When a single flanker is added (top right), the vernier  
173 reconstruction deteriorates (crowding) because the vernier is not well segmented from the flanker. When identical flank-  
174 ers are added (bottom left), the vernier reconstruction recovers, i.e., it is well segmented from the flankers (uncrowding).  
175 With different flankers (bottom right), the vernier is not represented at all in the two winning capsules (crowding). Inter-  
176 estingly, when the network produces “unexpected” uncrowding (i.e., the network shows uncrowding contrary to humans;  
177 bottom left), the reconstructions strongly resemble the case of “normal” uncrowding (compare middle and bottom left  
178 panels). In this case, the network was unable to notice the difference between circles and hexagons, and treated both  
179 stimuli in the same way. **c. Segmentation and (un)crowding in CapsNets:** If CapsNets can segment the vernier target away  
180 from the flankers during the recurrent routing by agreement process, uncrowding occurs. Segmentation is difficult when  
181 a single flanker surrounds the target because capsules disagree about what is shown at this location. In the case of con-  
182 figurations that the network has learned to group, many primary capsules agree about the presence of a group of shapes,  
183 which can therefore easily be segmented away from the vernier target.

184

185 In previous work, we have shown that pretrained ffCNNs (including an ffCNN biased towards global  
186 shape processing; 14) cannot explain uncrowding (18). Currently, CapsNets cannot be trained on  
187 large-scale tasks such as ImageNet because routing by agreement is computationally too expensive.  
188 Therefore, here, we took a different approach. As explained above, we trained our CapsNets to rec-  
189 cognize groups of shapes and verniers and asked how they would generalize from shapes presented in  
190 isolation to crowded shapes. To make sure that CapsNets explain global (un)crowding thanks to their  
191 grouping and segmentation *architecture* and not merely due to this different *training* regime, we con-  
192 ducted three further experiments. We investigated how performance changes when the capsule lay-  
193 ers are replaced by other architectures, keeping the number of neurons constant.

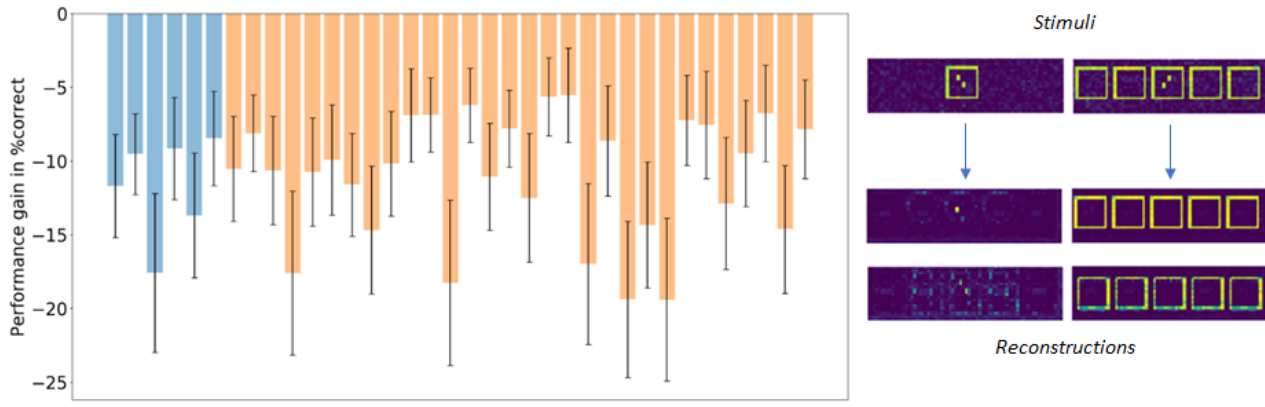
194 First, we replaced the capsules by a fully connected feedforward layer, yielding a classic ffCNN with  
195 three convolutional layers and a fully connected layer. We trained and tested this architecture exactly  
196 in the same way as the CapsNets, i.e., with the same stimuli, the same loss function, etc. The results  
197 clearly show that there is no uncrowding (Figure 3a): ffCNNs do not reproduce human-like global  
198 computations with this procedure.

199 Second, we added lateral recurrent connections to the fully connected layer of the previous ffCNN,  
200 yielding a network with three convolutional layers followed by a fully connected recurrent layer. We  
201 used the same number of recurrent iterations as for the routing by agreement in the CapsNets. Again,

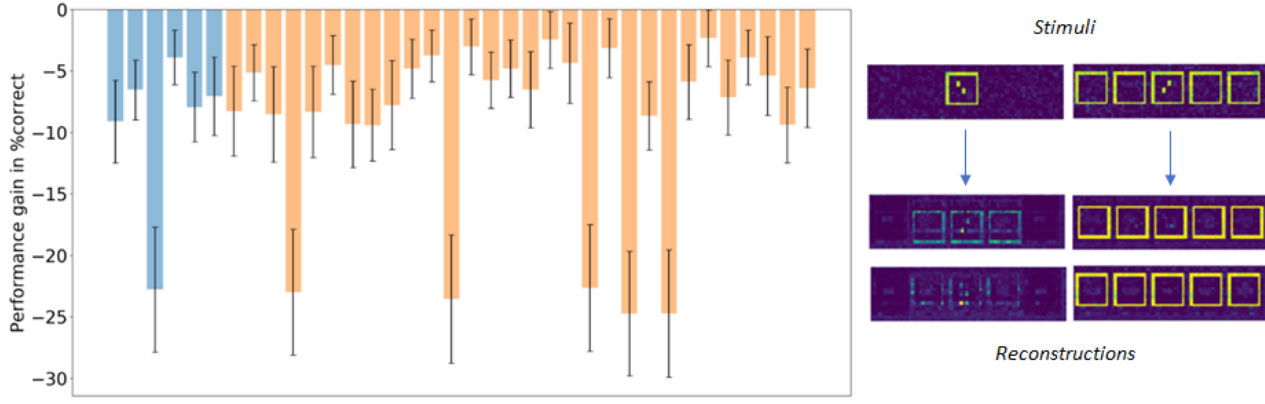
202 we trained and tested this architecture exactly like we trained and tested the CapsNets. There is no  
203 uncrowding with this architecture either (Figure 3b).

204 Lastly, we added top-down connections feeding back from the final fully connected layer of the pre-  
205 vious ffCNN to the layer below, yielding a network with three convolutional layers followed by a fully  
206 connected layer that fed back into the layer below (again with the same number of recurrent itera-  
207 tions as iterations of routing by agreement in the CapsNets). Again, after training and testing this  
208 architecture in the same way as the other networks, we found no uncrowding (Figure 3c). The absence  
209 of uncrowding in feedforward ffCNNs and ffCNNs with added lateral or top-down connections sug-  
210 gests that the *architecture* of CapsNets, and not our training regime, explains why (un)crowding is  
211 reproduced. Furthermore, recurrence by itself is not sufficient to produce (un)crowding. The grouping  
212 and segmentation performed by routing by agreement seems crucial.

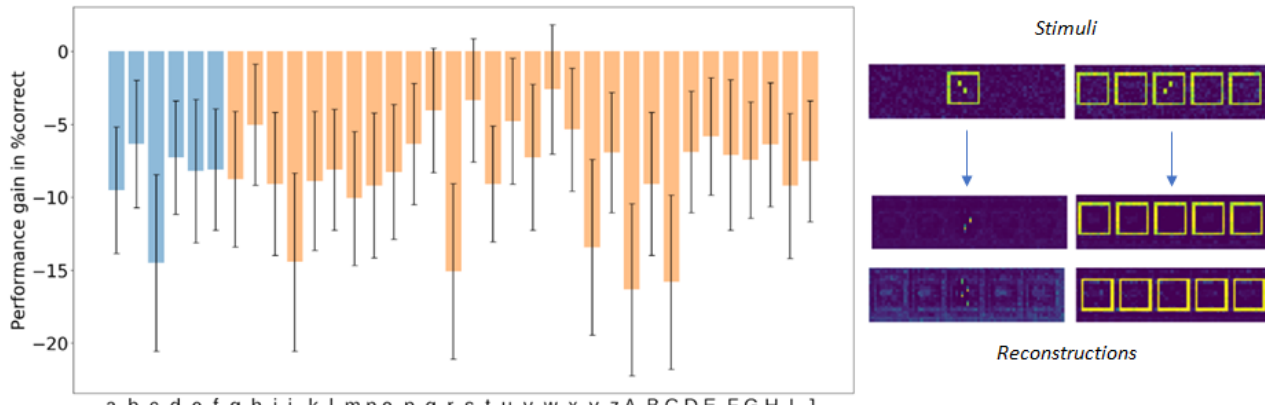
a. Feedforward CNN



b. CNN with added lateral recurrent connections



c. CNN with added top-down recurrent connections



213

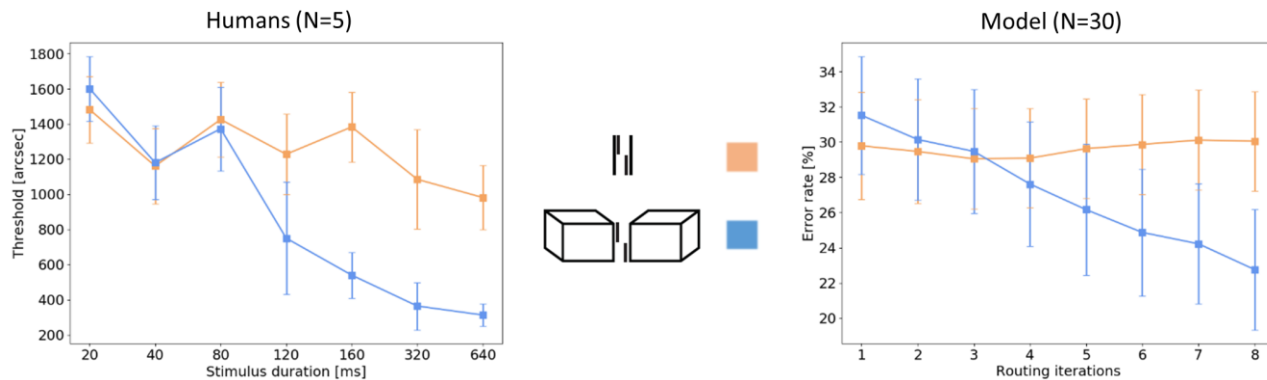
214 **Figure 3: Other network architectures do not explain uncrowding.** To verify that the ability of CapsNets to explain uncrowding  
 215 is due to their architecture and not merely to the way they are trained, we replaced the recurrent routing by agreement  
 216 processing by three different alternative architectures: a feedforward fully connected layer (yielding a classic ffCNN, a), a  
 217 fully connected layer with lateral recurrent connections (b) and a fully connected layer with top-down recurrent connec-  
 218 tions to the layer below (c). The plots on the left show the model's performance in the same way as figure 2a (the x-axes  
 219 represent (un)crowding stimuli, positive values on the y-axes show uncrowding). None of these architectures can produce  
 220 uncrowding (compare with the CapsNet results in figure 2a). On the right, reconstructions are shown. For all of these  
 221 networks, the vernier can be reconstructed with a single flanker but not when there are five flankers, showing that adding  
 222 further flanker increases crowding, in contrast to humans where adding flankers rescues perception of the vernier (un-  
 223 crowding).

224 Experiment 2: The role of recurrent processing

225 As mentioned, processing in CapsNets starts with a feedforward sweep followed by recurrent routing  
226 by agreement to refine grouping and segmentation. We hypothesize that humans may use recurrent  
227 processing to efficiently implement grouping and segmentation. To test this hypothesis, we psycho-  
228 physically investigated the temporal dynamics of (un)crowding. We show that uncrowding is mediated  
229 by a time-consuming *recurrent* process in humans. When the target groups with the flankers, crowd-  
230 ing occurs immediately. In contrast, when the target and flankers form separate groups, time-con-  
231 suming recurrent computations are required to segment the flanker from the target. We successfully  
232 model these results with CapsNets.

233 First, we performed a psychophysical crowding experiment with a vernier target flanked by either two  
234 lines or two cuboids (see Methods; Figure 4). The stimuli were displayed for varying durations from  
235 20 to 640ms and five observers reported the vernier offset direction. For short stimulus durations,  
236 crowding occurred for both flanker types, i.e., thresholds increased for both the lines and cuboids  
237 conditions compared to the vernier alone condition (lines:  $p = 0.0017$ , cuboids:  $p = 0.0013$ , 2-tailed  
238 one-sample t-tests).

239 We quantified how performance changed with increasing stimulus duration by fitting a line  $y = ax +$   
240  $b$  to the data for each subject, and comparing the mean slope  $a$  across subjects with 0 in one-sample  
241 2-tailed t-tests. The performance on the lines condition did not significantly change with increasing  
242 stimulus duration ( $p = 0.057$ ). These results are in accordance with previous results which show that  
243 crowding varies very little with stimulus duration (41; but see 42, 43). With the flanking cuboids we  
244 found a different pattern of results: performance dramatically improves with stimulus duration ( $p =$   
245 0.0007). This improvement cannot be explained by local mechanisms, such as lateral inhibition (30,  
246 44) or pooling (45–47) since the inner flanking vertical lines are the same in the lines and cuboids.  
247 Hence, according to a local approach we should expect no difference in thresholds between the two  
248 flanking conditions.



249

250 **Figure 4: Temporal dynamics of uncrowding:** *Left: Human data.* For cuboid flankers, strong crowding occurs up to 100ms  
 251 of stimulus presentation, and then uncrowding gradually occurs for longer durations (i.e., performance improves; blue).  
 252 The x-axis shows different stimulus durations and the y-axis shows the corresponding thresholds (i.e., lower values indicate  
 253 better performance). Error bars indicate standard error. Uncrowding does not occur with single line flankers, even for long  
 254 stimulus durations (orange). We hypothesize that the cuboids are segmented from the vernier target through time-con-  
 255 suming recurrent processing (the line flankers are grouped with the target and cannot be segmented at all). *Right: Model*  
 256 *data.* CapsNets can explain these results by varying the number of recurrent routing by agreement iterations. The x-axis  
 257 shows different numbers of routing iterations during testing and the y-axis shows the corresponding error rates (i.e., lower  
 258 values indicate better performance). Error bars indicate standard deviation across 30 trained networks (see Methods).  
 259 Similarly to humans, both lines and cuboids lead to crowding with few routing by agreement iterations. Performance  
 260 increases with routing iterations only for the cuboids. This suggests that recurrent processing helps to compute and seg-  
 261 ment the complex cuboids, but the lines are immediately strongly grouped with the vernier and can never be segmented.  
 262 Hence, they do not benefit from the recurrent segmentation process.

263

264 Crucially, uncrowding occurred for the cuboid flankers only when stimulus durations were sufficiently  
 265 long (Figure 4). In contrast, the effect of the line flankers does not change over time. We propose that  
 266 these results reflect the time-consuming recurrent computations needed to segment the cuboid  
 267 flankers away from the target. Performance does not improve with the line flankers, because they are  
 268 too strongly grouped with the vernier target, so recurrent processing cannot segment them away.  
 269 We trained CapsNets with the same architecture as in experiment 1 to discriminate vernier offsets,  
 270 and to recognize lines, cuboids and scrambled cuboids (see Methods; the scrambled cuboids were  
 271 included only to prevent the network from classifying lines vs. cuboids simply based on the number  
 272 of pixels in the image). As in experiment 1, during training, each training sample contained one of the  
 273 shape types, and the network had to classify which shape type was present and to discriminate the  
 274 vernier offset direction. We used 8 routing by agreement iterations during training. As in experiment

275 1, verniers and flankers were never presented together during training (i.e., there were no  
276 (un)crowding stimuli).

277 After training, we tested the networks on (un)crowding stimuli, changing the number recurrent rout-  
278 ing by agreement iterations from one (leading to a purely feedforward regime) to 8 iterations (a highly  
279 recurrent regime; Figure 3). We found that CapsNets naturally explain the human results. Using the  
280 same statistical analysis as for humans, we found that with more iterations, the cuboids are better  
281 segmented from the target, and performance improves ( $p = 0.003$ ). On the other hand, the effect of  
282 the line flankers does not change over time ( $p = 0.64$ ). These results were not affected by small  
283 changes in network hyperparameters or loss terms (supplementary material). We did not compare  
284 these results with the ffCNN and recurrent networks used in experiment 1, because these networks  
285 produced no uncrowding at all.

286 These findings are explained by the recurrent routing by agreement process. With cuboids, capsules  
287 across an extended spatial region need to agree about the presence of a cuboid, which is then seg-  
288 mented into its own capsule. This complex process requires several recurrent iterations of the routing  
289 by agreement process. On the other hand, the lines are immediately strongly grouped with the vernier,  
290 so further iterations of routing by agreement do not achieve successful segmentation and, hence,  
291 cannot improve performance.

292

## 293 Discussion

294 Our results provide strong evidence that time-consuming recurrent grouping and segmentation is  
295 crucial for shape-level computations in both humans and artificial neural networks. We used  
296 (un)crowding as a psychophysical probe to investigate how the brain flexibly forms object  
297 representations. These results specifically target global, shape-level and time-consuming recurrent  
298 computations and constitute a well-controlled and difficult challenge for neural networks.

299 It is well known that humans can solve a number of visual tasks very quickly, presumably in a single  
300 feedforward pass of neural activity (48). ffCNNs are good models of this kind of visual processing (21,  
301 22, 49). However, many studies have shown that neural activities are not determined by the  
302 feedforward sweep alone, and recurrent activity affords a distinct processing regime to perform more  
303 in-depth time-consuming computations (9, 10, 50–53). Similarly, CapsNets naturally include both a  
304 fast feedforward and a time-consuming recurrent regime. When a single routing by agreement  
305 iteration is used, CapsNets are rapid feedforward networks that can accomplish many tasks, such as

306 vernier discrimination or recognizing simple shape types (e.g. circles vs. squares). With more routing  
307 iterations, a recurrent processing regime arises and complex global shape effects emerge, such as  
308 segmenting the cuboids in experiment 2. We showed how the transition from feedforward to  
309 recurrent processing in CapsNets explains psychophysical results about temporal dynamics of  
310 (un)crowding.

311 Recurrent activity offers several advantages. First, although feedforward networks can in principle  
312 implement any function (54), recurrent networks can implement certain functions more efficiently.  
313 Flexible grouping and segmentation is exactly the kind of function that may benefit from recurrent  
314 computations (see also Seijdel et al., under review). For example, to determine which local elements  
315 should be grouped into a global object, it helps to compute this global object first. This information  
316 can then be fed back to influence how each local element is processed. For example, to model  
317 (un)crowding, it helps to compute the global configuration of flankers first to determine how to  
318 process the vernier. Should it be grouped with the flankers (crowding) or not (uncrowding)? In  
319 CapsNets, the first feedforward sweep of activity provides an initial guess about which global objects  
320 are present (e.g., large cuboids). At this stage, as shown in experiment 2, information about the  
321 vernier interferes with information about the cuboids (crowding). Then, recurrent processing routes  
322 information relative to cuboids and the vernier to different capsules (uncrowding). Without  
323 recurrence, in contrast, it is difficult to rescue the vernier information once it has been crowded.

324 Second, although any network architecture can implement any computation in principle (given  
325 enough neurons), they differ in the way they *generalize* to previously unseen stimuli. Hence, recurrent  
326 grouping and segmentation architectures influence what is learned from training data. Here, we have  
327 shown that only CapsNets, but not ffCNN or ffCNNs augmented with recurrent lateral or top-down  
328 connections, produce uncrowding when trained identically to recognize groups of shapes and verniers.  
329 In general, ffCNNs tend to generalize poorly (review: 55). Using different architectures to improve  
330 how current systems generalize is a promising avenue of research. In this respect, we have shown  
331 that CapsNets generalize more similarly to humans than ffCNNs and standard recurrent networks in  
332 the context of global (un)crowding.

333 One limitation in our experiments is that we explicitly taught the CapsNets which configurations to  
334 group together by selecting which groups of shapes were present during training (e.g., only groups of  
335 identical shapes in experiment 1). Effectively, this gave the network adequate priors to produce un-  
336 crowding with the appropriate configurations (i.e., only identical, but not different flankers). Hence,  
337 our results show that, given adequate priors, CapsNets explain uncrowding. We have shown that

338 ffCNNs and lateral or top-down recurrent connections do *not* produce uncrowding, *even* when they  
339 are trained identically on groups of identical shapes and showed learning on the training data com-  
340 parable to the CapsNets (furthermore, we showed previously that pretrained ffCNNs who are often  
341 used as general models of vision do not show uncrowding either; 18). This shows that merely training  
342 networks on groups of identical shapes is not sufficient to explain uncrowding. It is the recurrent seg-  
343 mentation in CapsNets that is crucial. Humans do not start from zero and therefore do not need to  
344 be trained in order to perform crowding tasks. The human brain is shaped through evolution and  
345 learning to group elements in a useful way to solve the tasks it faces. As mentioned, (un)crowding can  
346 be seen as a probe into this grouping strategy. Hence, we expect that training CapsNets on more  
347 naturalistic tasks such as ImageNet may lead to grouping strategies similar to humans and may there-  
348 fore naturally equip the networks with priors that explain (un)crowding results. At the moment, how-  
349 ever, CapsNets have not been trained on such difficult tasks because the routing by agreement algo-  
350 rithm is computationally too expensive.

351 Recurrent networks are harder to train than feedforward systems, which explains the dominance of  
352 the latter during these early days of deep learning. However, despite this hurdle, recurrent networks  
353 are emerging to address the limitations of ffCNNs as models of the visual system (10, 50, 52, 53, 56,  
354 57). Although there is consensus that recurrence is important for brain computations, it is currently  
355 unclear which functions exactly are implemented recurrently, and how they are implemented. Our  
356 results suggest that one important role of recurrence is shape-level computations through grouping  
357 and segmentation. We had previously suggested another recurrent segmentation network, hard-  
358 wired to explain uncrowding (58). However, CapsNets, bringing together recurrent grouping and seg-  
359 mentation with the power of deep learning, are much more flexible and can be trained to solve any  
360 task. Linsley et al. (53) proposed another recurrent deep neural network for grouping and segmenta-  
361 tion, and there are other possibilities too (59, 60). We do not suggest that CapsNets are the only  
362 implementation of grouping and segmentation. We only suggest that grouping and segmentation is  
363 important and further work is needed to show how the brain implements it.

364 In conclusion, our results provide mutually reinforcing modelling and psychophysical evidence that  
365 time-consuming, recurrent grouping and segmentation plays a crucial role for global shape  
366 computations in humans and machines.

367

## 368 Methods

369 The code to reproduce all our results will be available with the journal version of this contribution.

370 All models were implemented in Python 3.6, using the high-level estimator API of Tensorflow 1.10.0.

371 Computations were run on a GPU (NVIDIA GeForce GTX 1070). We used the same basic network

372 architecture in all experiments (Figure 5a). We implemented early feature extraction by using three

373 convolutional layers without padding, each followed by an ELU non-linearity. We used dropout (61)

374 after the first and second convolutional layers. The outputs of the last convolution were reshaped into

375  $m$  primary capsule types outputting  $n$ -dimensional activation vectors. The number of output capsule

376 types was equal to the number of different shapes used as input. The network was trained end-to-

377 end through backpropagation. For training, we used an Adam optimizer with a batch size of 48 and a

378 learning rate of 0.0004. To this learning rate, we applied cosine decays with warm restarts (62).

379 This choice of network architecture was motivated by the following rationale (Figure 5b). After

380 training, ideally, primary capsules detect the individual shapes present in the input image, and output

381 capsules group and segment these shapes through recurrent routing by agreement. The network can

382 only group shapes together if it was taught during training that these shapes should form a group. To

383 match this rationale, we set the primary capsules' receptive field sizes to roughly the size of one shape,

384 and we set the number of output capsules equal to the number of shape types.

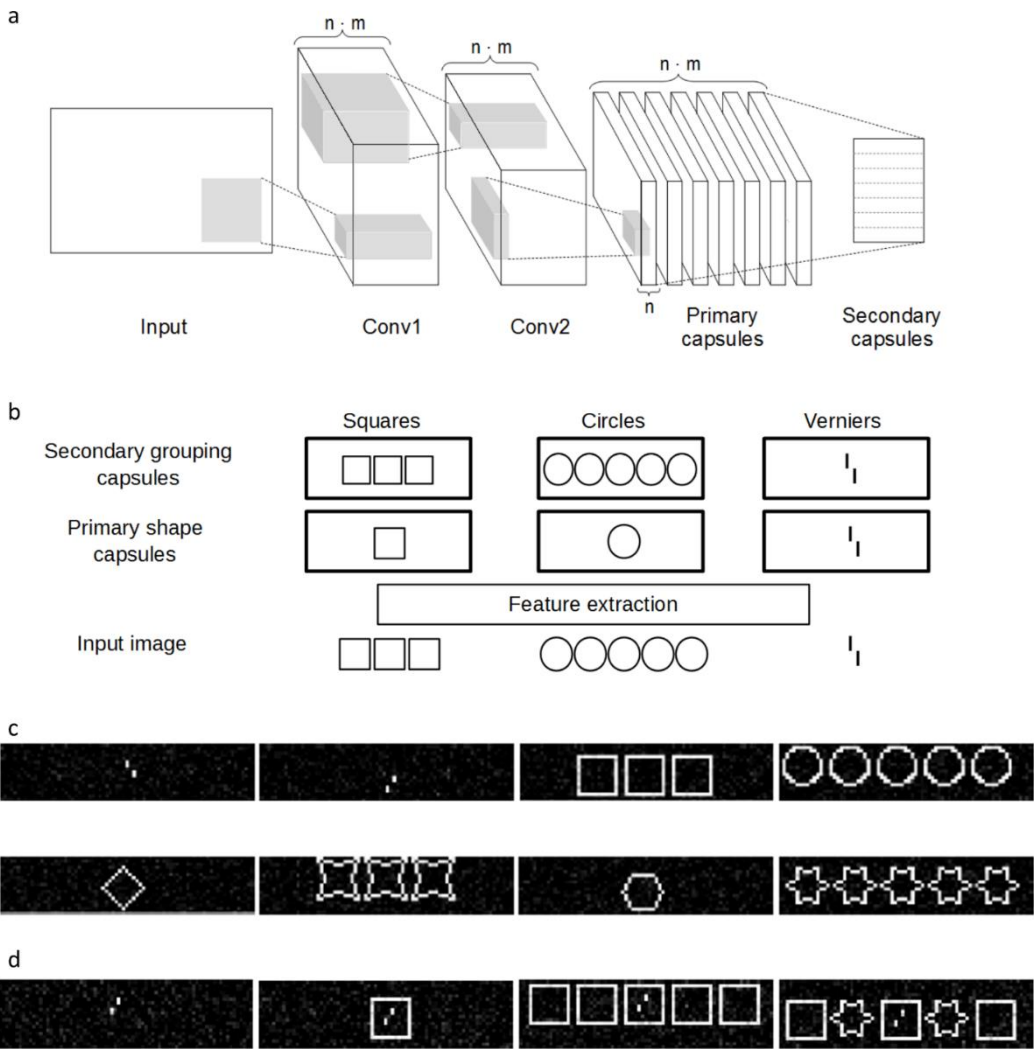
385 Inputs were grayscale images (Figure 5c&d). We added random Gaussian noise with mean  $\mu = 0$  and

386 standard deviation randomly drawn from a uniform distribution  $\sigma \sim \mathcal{U}(0.00, 0.02)$ . The contrast was

387 varied either by first adding a random value between -0.1 and 0.1 to all pixel values and then

388 multiplying them with a random value drawn from a uniform distribution  $\mathcal{U}(0.6, 1.2)$ , or vice versa.

389 The pixel values were then clipped between 0 and 1.



390

391 **Figure 5: a. Network architecture:** We used capsule networks with three convolutional layers whose last outputs was  
 392 reshaped into the primary capsule layer with  $m$  primary capsule types and  $n$  primary capsule dimensions. In this example,  
 393 the number of primary and output capsules types is seven to match the seven shape types we used in experiment 1 (see  
 394 caption c), but the number depended on the experiment. The primary and output capsule layers communicate via routing-  
 395 by-agreement. **b. Ideal representations:** After training, the primary capsules detect single shapes of different types at  
 396 different locations. In this example, there are squares, circles and verniers. By routing the outputs of the primary capsules  
 397 to the corresponding output capsules, the output capsules group these shapes in groups of one, three or five, based on  
 398 the number of shapes detected by the primary capsules. If the left stimulus with three squares is presented, the primary  
 399 square capsules detect squares at three different locations. Through routing by agreement, the output squares capsule  
 400 groups these three squares. If the middle stimulus with five circles is presented, the primary circle capsules detect circles  
 401 at five different locations. Through routing by agreement, the output circles capsule represents a group of five circles after  
 402 routing. Lastly, if a vernier is presented (right stimulus), it is detected by primary capsules and is represented in the vernier  
 403 output capsule. **c. Training stimuli for experiment 1:** All shapes were shown randomly in groups of one, three or five, except  
 404 verniers who were always presented alone. **d. Testing stimuli for experiment 1:** Example stimuli for the four test conditions:  
 405 In the vernier-alone condition (*left*), we expected the network to perform well on the vernier discrimination task. In  
 406 crowding conditions (*middle-left*), we expected a deterioration of the vernier discrimination as in classical crowding. In  
 407 uncrowding conditions with many identical flankers (*middle-right*), we expected a recovery of the vernier discrimination.

408 In no-uncrowding conditions with different flanker types (*right*), we expected crowding. After training, the network has  
409 learnt about groups of identical shapes and verniers, but has never encountered these (un)crowding stimuli.

410

411 **Experiment 1:**

412 **Modelling**

413 Human data for experiment 1 is based on (26). We trained CapsNets with the above architecture to  
414 solve a vernier offset discrimination task and classify groups of identical shapes. The training dataset  
415 included vernier stimuli and six different shape types (Figure 4c). Shapes were presented in groups of  
416 one, three or five shapes of the same type. The group was centered in the middle of the image, with  
417 a jitter of 2 pixels along the x-axis and 6 pixels along the y-axis.

418 The loss function included a term for shape type classification, a term for vernier offset discrimination,  
419 a term for the number of shapes in the image, and a term for reconstructing the input based on the  
420 network output (see equations 1-5). Each loss term was scaled so that none of the terms dominated  
421 the others. For the shape type classification loss, we implemented the same margin loss as in (2). This  
422 loss enables the detection of multiple objects in the same image. For the vernier offset loss, we used  
423 a small decoder to determine vernier offset directions based on the activity of the vernier output  
424 capsule. The decoder was composed of a single dense hidden layer followed by a ReLU-nonlinearity  
425 and a dense readout layer of two nodes corresponding to the labels left and right. The vernier offset  
426 loss was computed as the softmax cross entropy between the decoder output and the one-hot-en-  
427 coded vernier offset labels. The loss term for the number of shapes in the image was implemented  
428 similarly, but the output layer comprised three nodes representing the labels one, three or five shape  
429 repetitions. For the reconstruction loss, we trained a decoder with two fully-connected hidden layers  
430 (h1: 512 units, h2: 1024 units) each followed by ELU nonlinearities to reconstruct the input image.  
431 The reconstruction loss was then calculated as the squared difference between the pixel values of the  
432 input image and the reconstructed image. The total loss is given by the following formulas:

$$433 \quad L_{total} = \alpha_{shape\ type} L_{shape\ type} + \alpha_{vernier\ offset} L_{vernier\ offset} \\ 434 \quad + \alpha_{shape\ repetitions} L_{shape\ repetitions} + \alpha_{reconstruction} L_{reconstruction} \quad (1)$$

$$435 \quad L_{shape\ type} = \sum_k T_k \max(0, (m^+ - \|v_k\|)^2) + \lambda(1 - T_k) \max(0, (\|v_k\| - m^-)^2) \quad (2)$$

$$436 \quad L_{vernier\ offset} = \text{Crossentropy}(\text{vernier labels}, \text{vernier decoder output}) \quad (3)$$

$$437 \quad L_{shape\ repetitions} \\ 438 \quad = \text{Crossentropy}(\text{shape repetitions labels}, \text{shape repetitions decoder output}) \quad (4)$$

439 
$$L_{reconstruction} = \sum_{i,j} (input(i,j) - reconstruction(i,j))^2 \quad (5)$$

440 Where the  $\alpha$  are real numbers scaling each loss term,  $T_k = 1$  if shape class  $k$  is present,  $\|v_k\|$  is the  
441 norm of output capsule  $k$ , and  $m^+$ ,  $m^-$  and  $\lambda$  are parameters of the margin loss with the same values  
442 as described in (2).

443 After training, we tested vernier discrimination performance on (un)crowding stimuli (figure 4d), and  
444 obtained input reconstructions. We trained 10 different networks and averaged their performance.  
445 Before this experiment, the network had never seen crowding nor uncrowding stimuli, but it knew  
446 about groups of shapes and about the vernier discrimination task. Therefore, the network could not  
447 trivially learn when to (un)crowd by overfitting on the training dataset. This situation is similar for  
448 humans: they know about shapes and verniers, but their visual system has never been trained on  
449 (un)crowding stimuli.

450 To check that CapsNets explain uncrowding because of the grouping and segmentation capabilities  
451 offered by routing by agreement and not merely because of the way they are trained, we replaced  
452 the capsule layers by other architectures (a feedforward fully connected layer, a fully connected layer  
453 with lateral recurrent connections and a fully connected layer with top-down recurrent connections  
454 to the layer below; see Results). All these networks had the same number of neurons as our CapsNets,  
455 and we used the same number of recurrent iterations as the number of routing by agreement used  
456 for the CapsNets. The networks were trained and tested in exactly the same way, with the same losses  
457 and datasets. The only difference is that CapsNets represent different classes in different capsules, so  
458 we could decode information directly from specific capsules (for example, we could decode vernier  
459 offsets specifically from the vernier capsule, or reconstruct squares specifically from the squares cap-  
460 sule). The other networks do not offer this possibility, because different classes are not represented  
461 in different known groups of neurons. Therefore, we decoded vernier offsets, reconstructions, the  
462 number of shapes and the shape type from the entire last layer of the network rather than from  
463 specific capsules. This difference did not limit the networks' performance, since these architectures  
464 performed well during training. Hence, the fact that they do not produce uncrowding is not explained  
465 by training limitations, but rather by the fact that they *generalize* to novel inputs differently than Cap-  
466 sNets.

467

468 **Experiment 2:**

469 **Psychophysical experiment:**

470 *Observers*

471 For experiment 2, we collected human psychophysical data. Participants were paid students of the  
472 Ecole Polytechnique Fédérale de Lausanne (EPFL). All had normal or corrected-to-normal vision, with  
473 a visual acuity of 1.0 (corresponding to 20/20) or better in at least one eye, measured with the Frei-  
474 burg Visual Acuity Test. Observers were told that they could quit the experiment at any time they  
475 wished. Five observers (two females) performed the experiment.

476 *Apparatus and stimuli*

477 Stimuli were presented on a HP-1332A XY-display equipped with a P11 phosphor and controlled by a  
478 PC via a custom-made 16-bit DA interface. Background luminance of the screen was below 1 cd/m<sup>2</sup>.  
479 Luminance of stimuli was 80 cd/m<sup>2</sup>. Luminance measurements were performed using a Minolta Lu-  
480 minance meter LS-100. The experimental room was dimly illuminated (0.5 lx). Viewing distance was  
481 75 cm.

482 We determined vernier offset discrimination thresholds for different flanker configurations. The ver-  
483 nier target consisted of two lines that were randomly offset either to the left or right. Observers indi-  
484 cated the offset direction. Stimulus consisted of two vertical 40' (arcmin) long lines separated by a  
485 vertical gap of 4' and presented at an eccentricity of 5° to the right of a fixation cross (6' diameter).  
486 Eccentricity refers to the center of the target location. Flanker configurations were centered on the  
487 vernier stimulus and were symmetrical in the horizontal dimension. Observers were presented two  
488 flanker configurations. In the lines configuration, the vernier was flanked by two vertical lines (84') at  
489 40' from the vernier. In the cuboids configuration, perspective cuboids were presented to the left and  
490 to the right of the vernier (width = 58', angle of oblique lines = 135°, length = 23.33'). Cuboids con-  
491 tained the lines from the Lines condition as their centermost edge.

492 *Procedure*

493 Observers were instructed to fixate a fixation cross during the trial. After each response, the screen  
494 remained blank for a maximum period of 3 s during which the observer was required to make a re-  
495 sponse on vernier offset discrimination by pressing one of two push buttons. The screen was blank  
496 for 500 ms between response and the next trial.

497 An adaptive staircase procedure (PEST; 63) was used to determine the vernier offset for which ob-  
498 servers reached 75% correct responses. Thresholds were determined after fitting a cumulative Gauss-  
499 ian to the data using probit and likelihood analyses. In order to avoid extremely large vernier offsets,

500 we restricted the PEST procedure to not exceed 33.3' i.e. twice the starting value of 16.66'. Each condition  
501 was presented in separate blocks of 80 trials. All conditions were measured twice (i.e., 160  
502 trials) and randomized individually for each observer. To compensate for possible learning effects, the  
503 order of conditions was reversed after each condition had been measured once. Auditory feedback  
504 was provided after incorrect or omitted responses.

505 **Modelling:**

506 To model the results of experiment 2, we trained our CapsNets to solve a vernier offset discrimination  
507 task and classify verniers, cuboids, scrambled cuboids and lines. The training dataset included vernier  
508 stimuli and one of three different shape types (lines, cuboids, scrambled cuboids). The scrambled  
509 cuboids were included to make the task harder, and to prevent the network from classifying cuboids  
510 simply based on the number of pixels in the image. The line stimuli were randomly presented in a  
511 group of 2, 4, 6 or 8. Both, cuboids and shuffled cuboids were always presented in groups of two  
512 facing one another. The distance between these shapes was varied randomly between one and six  
513 pixels. The loss function was very similar to experiment 1, but without the loss term for shape repeti-  
514 tions, since there were no repetitions (each term is the same as in eqs. 1-5):

515 
$$L_{total} = \alpha_{shape\ type} L_{shape\ type} + \alpha_{vernier\ offset} L_{vernier\ offset} + \alpha_{reconstruction} L_{reconstruction} \quad (6)$$

516 After training, we tested the network's vernier discrimination performance on (un)crowding stimuli  
517 (verniers surrounded by either lines, cuboids or scrambled cuboids), while varying the number of  
518 recurrent routing by agreement iterations. We trained the same network 50 times and averaged per-  
519 formance over these trained networks, excluding 21 networks for which vernier discrimination per-  
520 formance with *both* line and cuboid flankers was at ceiling ( $\geq 95\%$ ) or floor ( $\leq 55\%$ ). This exclusion  
521 criterion is used for cleaner results and does *not* impact the crucial result showing that uncrowding  
522 occurs with increasing routing iterations only with cuboid, but not with line flankers. The effect still  
523 occurs when all 50 networks are included in the analysis, but the fact that certain networks are at  
524 floor or ceiling is misleading. Before this experiment, the network had never seen (un)crowding stim-  
525 uli, but it knew about cuboids, scrambled cuboids and about the vernier discrimination task. There-  
526 fore, the network could not trivially learn when to (un)crowd by overfitting on the training dataset.

527

528 **Acknowledgements**

529 Adrien Doerig was supported by the Swiss National Science Foundation grant n.176153 "Basics of  
530 visual processing: from elements to figures".

531

532 **Bibliography**

- 533 1. A. Doerig, *et al.*, Beyond Bouma's window: How to explain global aspects of crowding? *PLOS*  
534 *Computational Biology* **15**, e1006580 (2019).
- 535 2. S. Sabour, N. Frosst, G. E. Hinton, Dynamic routing between capsules in *Advances in Neural*  
536 *Information Processing Systems*, (2017), pp. 3856–3866.
- 537 3. J. J. DiCarlo, D. Zoccolan, N. C. Rust, How Does the Brain Solve Visual Object Recognition?  
538 *Neuron* **73**, 415–434 (2012).
- 539 4. D. H. Hubel, T. N. Wiesel, Receptive fields, binocular interaction and functional architecture in  
540 the cat's visual cortex. *The Journal of physiology* **160**, 106–154 (1962).
- 541 5. A. Krizhevsky, I. Sutskever, G. E. Hinton, Imagenet classification with deep convolutional neural  
542 networks in *Advances in Neural Information Processing Systems*, (2012), pp. 1097–1105.
- 543 6. S. A. Eslami, *et al.*, Neural scene representation and rendering. *Science* **360**, 1204–1210 (2018).
- 544 7. L. Gatys, A. S. Ecker, M. Bethge, “Texture Synthesis Using Convolutional Neural Networks” in  
545 *Advances in Neural Information Processing Systems 28*, C. Cortes, N. D. Lawrence, D. D. Lee, M.  
546 Sugiyama, R. Garnett, Eds. (Curran Associates, Inc., 2015), pp. 262–270.
- 547 8. T. Karras, S. Laine, T. Aila, A style-based generator architecture for generative adversarial  
548 networks. *arXiv preprint arXiv:1812.04948* (2018).
- 549 9. V. A. Lamme, P. R. Roelfsema, The distinct modes of vision offered by feedforward and recurrent  
550 processing. *Trends in neurosciences* **23**, 571–579 (2000).
- 551 10. T. C. Kietzmann, *et al.*, Recurrence required to capture the dynamic computations of the human  
552 ventral visual stream. *arXiv preprint arXiv:1903.05946* (2019).
- 553 11. C. M. Funke, *et al.*, Comparing the ability of humans and DNNs to recognise closed contours in  
554 cluttered images in *18th Annual Meeting of the Vision Sciences Society (VSS 2018)*, (2018), p.  
555 213.
- 556 12. J. Su, D. V. Vargas, K. Sakurai, One pixel attack for fooling deep neural networks. *IEEE*  
557 *Transactions on Evolutionary Computation* (2019).
- 558 13. C. Szegedy, *et al.*, Intriguing properties of neural networks. *arXiv preprint arXiv:1312.6199*  
559 (2013).
- 560 14. R. Geirhos, *et al.*, ImageNet-trained CNNs are biased towards texture; increasing shape bias  
561 improves accuracy and robustness. *arXiv preprint arXiv:1811.12231* (2018).
- 562 15. N. Baker, H. Lu, G. Erlikhman, P. J. Kellman, Deep convolutional networks do not classify based  
563 on global object shape. *PLoS computational biology* **14**, e1006613 (2018).
- 564 16. W. Brendel, M. Bethge, Approximating CNNs with Bag-of-local-Features models works  
565 surprisingly well on ImageNet. *arXiv preprint arXiv:1904.00760* (2019).

566 17. T. Kim, W. Bair, A. Pasupathy, Neural coding for shape and texture in macaque area V4. *Journal of*  
567 *Neuroscience* **39**, 4760–4774 (2019).

568 18. A. Doerig, A. Bornet, O. H. Choung, M. H. Herzog, Crowding Reveals Fundamental Differences in  
569 Local vs. Global Processing in Humans and Machines. *bioRxiv*, 744268 (2019).

570 19. K. Hermann, S. Kornblith, Exploring CNN Inductive Biases: Shape vs. Texture. *NeurIPS Workshop*  
571 *on Shared Visual Representations in Human & Machine Intelligence* (2019).

572 20. J. Deng, *et al.*, Imagenet: A large-scale hierarchical image database in 2009 *IEEE Conference on*  
573 *Computer Vision and Pattern Recognition*, (Ieee, 2009), pp. 248–255.

574 21. S.-M. Khaligh-Razavi, N. Kriegeskorte, Deep supervised, but not unsupervised, models may  
575 explain IT cortical representation. *PLoS computational biology* **10**, e1003915 (2014).

576 22. D. L. Yamins, *et al.*, Performance-optimized hierarchical models predict neural responses in  
577 higher visual cortex. *Proceedings of the National Academy of Sciences* **111**, 8619–8624 (2014).

578 23. B. RichardWebster, S. Anthony, W. Scheirer, Psyphy: A psychophysics driven evaluation  
579 framework for visual recognition. *IEEE transactions on pattern analysis and machine intelligence*  
580 (2018).

581 24. D. M. Levi, Crowding—An essential bottleneck for object recognition: A mini-review. *Vision*  
582 *Research* **48**, 635–654 (2008).

583 25. D. Whitney, D. M. Levi, Visual crowding: a fundamental limit on conscious perception and object  
584 recognition. *Trends in Cognitive Sciences* **15**, 160–168 (2011).

585 26. H. Bouma, Visual interference in the parafoveal recognition of initial and final letters of words.  
586 *Vision Research* **13**, 767–782 (1973).

587 27. D. G. Pelli, Crowding: a cortical constraint on object recognition. *Current Opinion in*  
588 *Neurobiology* **18**, 445–451 (2008).

589 28. M. Manassi, D. Whitney, Multi-level Crowding and the Paradox of Object Recognition in Clutter.  
590 *Current Biology* **28**, R127–R133 (2018).

591 29. M. Manassi, S. Lonchampt, A. Clarke, M. H. Herzog, What crowding can tell us about object  
592 representations. *Journal of Vision* **16**, 35–35 (2016).

593 30. G. Westheimer, G. Hauske, Temporal and spatial interference with vernier acuity. *Vision research*  
594 **15**, 1137–1141 (1975).

595 31. D. M. Levi, S. A. Klein, A. P. Aitsebaomo, Vernier acuity, crowding and cortical magnification.  
596 *Vision research* **25**, 963–977 (1985).

597 32. D. Oberfeld, P. Stahn, Sequential grouping modulates the effect of non-simultaneous masking on  
598 auditory intensity resolution. *PloS one* **7**, e48054 (2012).

599 33. K. E. Overvliet, B. Sayim, Perceptual grouping determines haptic contextual modulation. *Vision*  
600 *Research* **126**, 52–58 (2016).

601 34. T. P. Saarela, B. Sayim, G. Westheimer, M. H. Herzog, Global stimulus configuration modulates  
602 crowding. *Journal of Vision* **9**, 5–5 (2009).

603 35. M. H. Herzog, M. Fahle, Effects of grouping in contextual modulation. *Nature* **415**, 433 (2002).

604 36. B. Sayim, G. Westheimer, M. H. Herzog, Gestalt factors modulate basic spatial vision.  
605 *Psychological Science* **21**, 641–644 (2010).

606 37. T. P. Saarela, G. Westheimer, M. H. Herzog, The effect of spacing regularity on visual crowding.  
607 *Journal of Vision* **10**, 17–17 (2010).

608 38. M. Manassi, B. Sayim, M. H. Herzog, Grouping, pooling, and when bigger is better in visual  
609 crowding. *Journal of Vision* **12**, 13–13 (2012).

610 39. M. V. Pachai, A. C. Doerig, M. H. Herzog, How best to unify crowding? *Current Biology* **26**, R352–  
611 R353 (2016).

612 40. M. Manassi, B. Sayim, M. H. Herzog, When crowding of crowding leads to uncrowding. *Journal*  
613 *of Vision* **13**, 10–10 (2013).

614 41. J. M. Wallace, M. K. Chiu, A. S. Nandy, B. S. Tjan, Crowding during restricted and free viewing.  
615 *Vision Research* **84**, 50–59 (2013).

616 42. S. P. Tripathy, P. Cavanagh, H. E. Bedell, Large crowding zones in peripheral vision for briefly  
617 presented stimuli. *Journal of Vision* **14**, 11–11 (2014).

618 43. E. A. Styles, D. A. Allport, Perceptual integration of identity, location and colour. *Psychological*  
619 *Research* **48**, 189–200 (1986).

620 44. Z. Li, Visual segmentation by contextual influences via intra-cortical interactions in the primary  
621 visual cortex. *Network: computation in neural systems* **10**, 187–212 (1999).

622 45. L. Parkes, J. Lund, A. Angelucci, J. A. Solomon, M. Morgan, Compulsory averaging of crowded  
623 orientation signals in human vision. *Nature neuroscience* **4**, 739 (2001).

624 46. D. G. Pelli, M. Palomares, N. J. Majaj, Crowding is unlike ordinary masking: Distinguishing feature  
625 integration from detection. *Journal of Vision* **4**, 12–12 (2004).

626 47. R. Rosenholtz, D. Yu, S. Keshvari, Challenges to pooling models of crowding: Implications for  
627 visual mechanisms. *Journal of vision* **19** (2019).

628 48. S. Thorpe, D. Fize, C. Marlot, Speed of processing in the human visual system. *nature* **381**, 520  
629 (1996).

630 49. T. C. Kietzmann, P. McClure, N. Kriegeskorte, Deep neural networks in computational  
631 neuroscience. *bioRxiv*, 133504 (2018).

632 50. J. Kim, D. Linsley, K. Thakkar, T. Serre, Disentangling neural mechanisms for perceptual grouping.  
633 *arXiv preprint arXiv:1906.01558* (2019).

634 51. H. Tang, *et al.*, Recurrent computations for visual pattern completion. *Proceedings of the*  
635 *National Academy of Sciences* **115**, 8835–8840 (2018).

636 52. C. J. Spoerer, T. C. Kietzmann, N. Kriegeskorte, Recurrent networks can recycle neural resources  
637 to flexibly trade speed for accuracy in visual recognition. *bioRxiv*, 677237 (2019).

638 53. D. Linsley, J. Kim, T. Serre, Sample-efficient image segmentation through recurrence.  
639 *arXiv:1811.11356 [cs]* (2018) (June 27, 2019).

640 54. K. Hornik, M. Stinchcombe, H. White, Multilayer feedforward networks are universal  
641 approximators. *Neural networks* **2**, 359–366 (1989).

642 55. T. Serre, Deep learning: the good, the bad, and the ugly. *Annual Review of Vision Science* **5**, 399–  
643 426 (2019).

644 56. C. J. Spoerer, P. McClure, N. Kriegeskorte, Recurrent convolutional neural networks: a better  
645 model of biological object recognition. *Frontiers in psychology* **8**, 1551 (2017).

646 57. K. Kar, J. Kubilius, K. Schmidt, E. B. Issa, J. J. DiCarlo, Evidence that recurrent circuits are critical to  
647 the ventral stream’s execution of core object recognition behavior. *Nature neuroscience* **22**, 974  
648 (2019).

649 58. G. Francis, M. Manassi, M. H. Herzog, Neural dynamics of grouping and segmentation explain  
650 properties of visual crowding. *Psychological review* **124**, 483 (2017).

651 59. O. Ronneberger, P. Fischer, T. Brox, U-net: Convolutional networks for biomedical image  
652 segmentation in *International Conference on Medical Image Computing and Computer-Assisted*  
653 *Intervention*, (Springer, 2015), pp. 234–241.

654 60. R. Girshick, I. Radosavovic, G. Gkioxari, P. Dollár, K. He, *Detectron* (2018).

655 61. N. Srivastava, G. Hinton, A. Krizhevsky, I. Sutskever, R. Salakhutdinov, Dropout: a simple way to  
656 prevent neural networks from overfitting. *The Journal of Machine Learning Research* **15**, 1929–  
657 1958 (2014).

658 62. I. Loshchilov, F. Hutter, Sgdr: Stochastic gradient descent with warm restarts. *arXiv preprint*  
659 *arXiv:1608.03983* (2016).

660 63. M. Taylor, C. D. Creelman, PEST: Efficient estimates on probability functions. *The Journal of the*  
661 *Acoustical Society of America* **41**, 782–787 (1967).

662

663

## 664 Supplementary Material

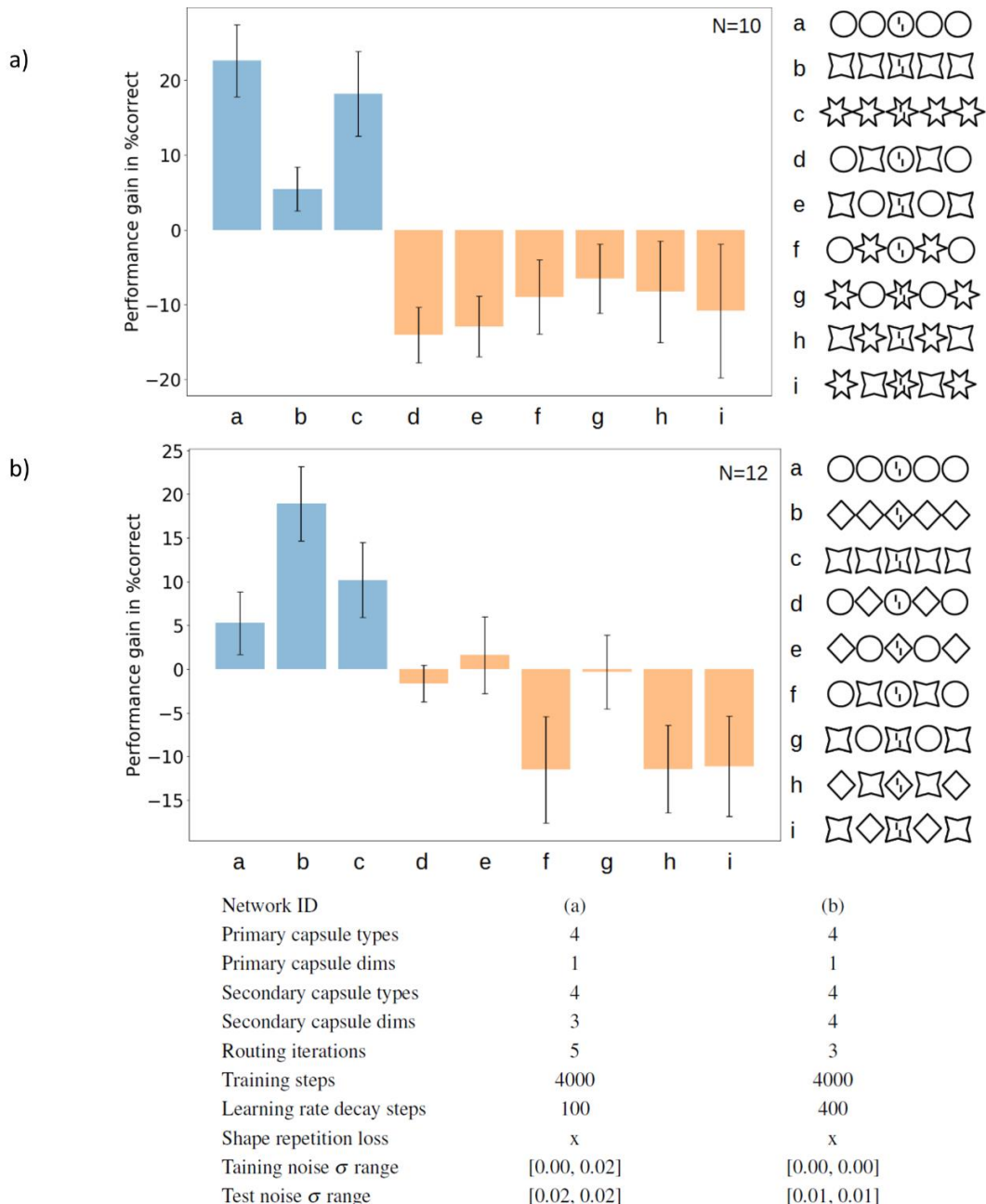
### 665 Experiment 1

#### 666 Results are robust against stimuli and hyperparameters changes

667 To avoid cherrypicking our hyperparameters, we ran several networks with different hyperparameter  
668 sets, and show that our results are robust with respect to these changes.

669 The results of experiment 1 remain qualitatively similar for different image sizes and network  
670 hyperparameters. Below is a selection of results using different sets of hyperparameters. In all these  
671 cases, both crowding and uncrowding occur, similarly to the results shown in Figure 2.

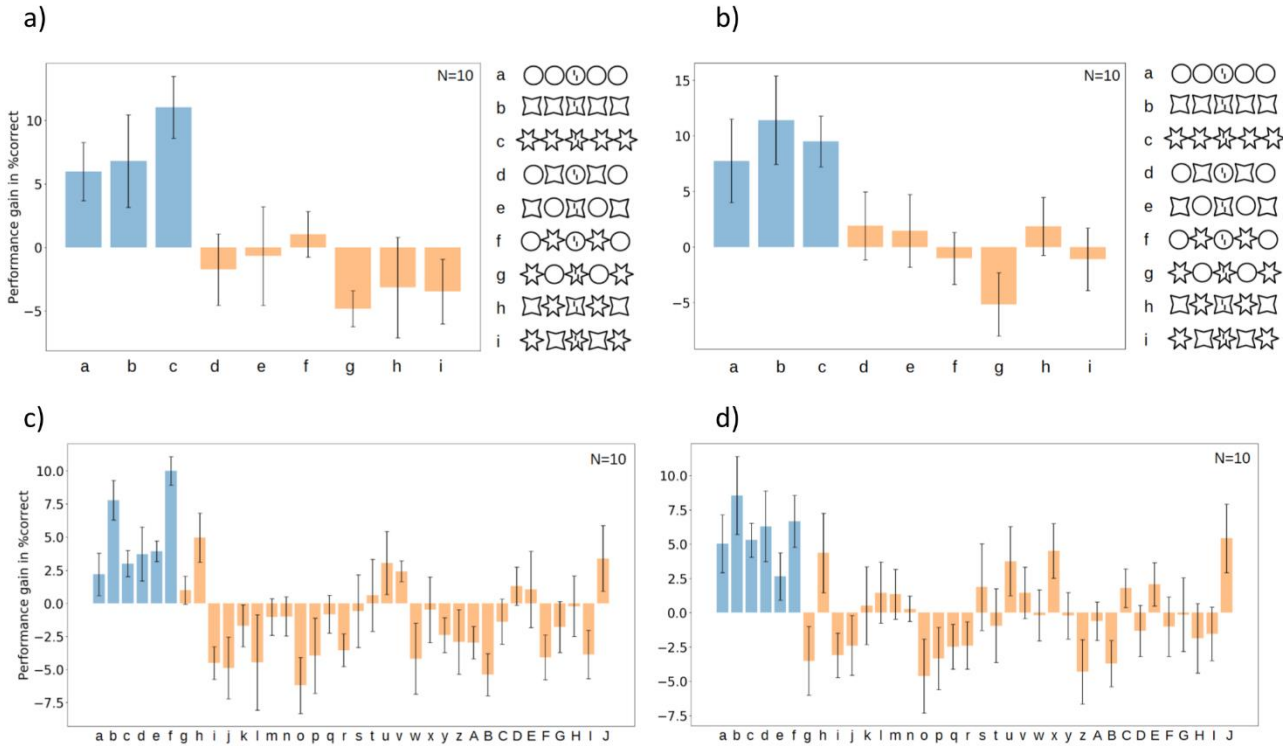
672



673

674 **Supplementary Figure 1: Results for 16x72 pixel images.** Both crowding and uncrowding occur similarly to the results in  
 675 figure 2. Plotting conventions are the same as in figure 2. Main hyperparameters are summarized at the bottom. With  
 676 these small images, we often encountered ceiling effects. We trained 20 networks and dropped those that were at  
 677 ceiling (i.e., we dropped networks that were at 100% performance for all conditions).

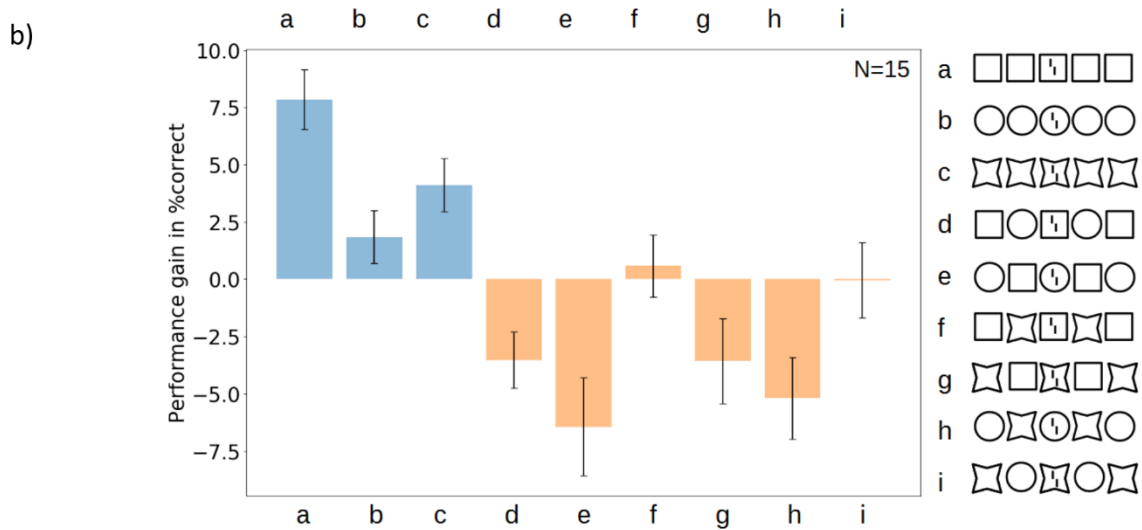
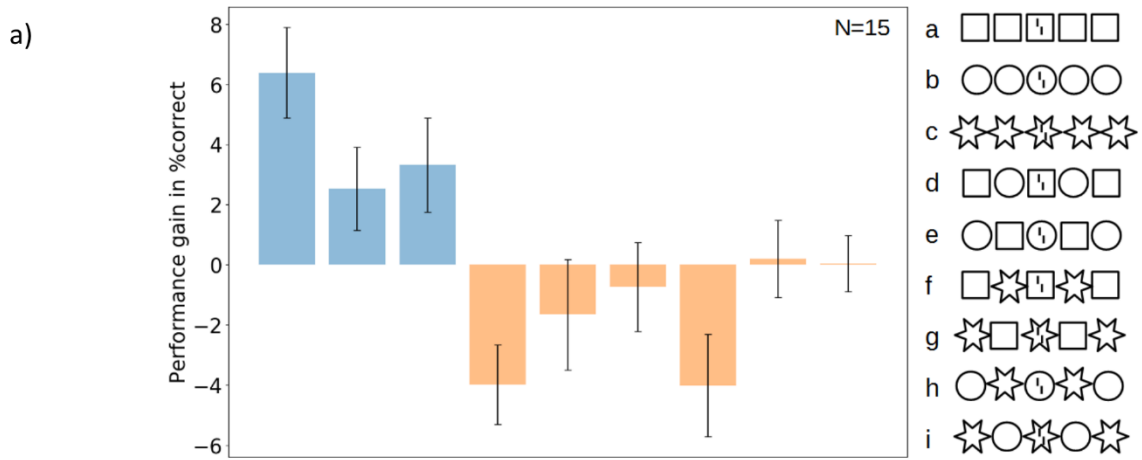
678



| Network ID              | (a)          | (b)          | (c)          | (d)          |
|-------------------------|--------------|--------------|--------------|--------------|
| Primary capsule types   | 4            | 4            | 7            | 7            |
| Primary capsule dims    | 1            | 1            | 2            | 2            |
| Secondary capsule types | 4            | 4            | 7            | 7            |
| Secondary capsule dims  | 4            | 4            | 8            | 10           |
| Routing iterations      | 3            | 5            | 3            | 3            |
| Training steps          | 8000         | 6000         | 2500         | 5000         |
| Shape repetition loss   | X            | X            | X            | X            |
| Location loss           |              |              | X            | X            |
| Reconstruction loss     |              |              | X            | X            |
| Gaussian training noise | [0.00, 0.05] | [0.00, 0.00] | [0.02, 0.04] | [0.02, 0.04] |
| Gaussian test noise     | [0.05, 0.05] | [0.05, 0.05] | [0.04, 0.06] | [0.04, 0.06] |

679

680 **Supplementary Figure 2: 20x72 pixel images.** Both crowding and uncrowding occur similarly to the results in figure 2.  
 681 Plotting conventions are the same as in figure 2. Main hyperparameters are summarized at the bottom. Stimuli not  
 682 shown for panels b&c, for clarity.



| Network ID              | (a)          | (b)          |
|-------------------------|--------------|--------------|
| Primary capsule types   | 20           | 20           |
| Primary capsule dims    | 1            | 1            |
| Secondary capsule types | 4            | 4            |
| Secondary capsule dims  | 12           | 12           |
| Routing iterations      | 4            | 5            |
| Training steps          | 3000         | 3000         |
| First decay steps       | 500          | 500          |
| Shape repetition loss   | x            | x            |
| Gaussian training noise | [0.00, 0.00] | [0.00, 0.02] |
| Gaussian test noise     | [0.01, 0.01] | [0.01, 0.01] |

683

684 **Supplementary Figure 3: 30x72 pixel images.** Both crowding and uncrowding occur similarly to the results in figure 2.

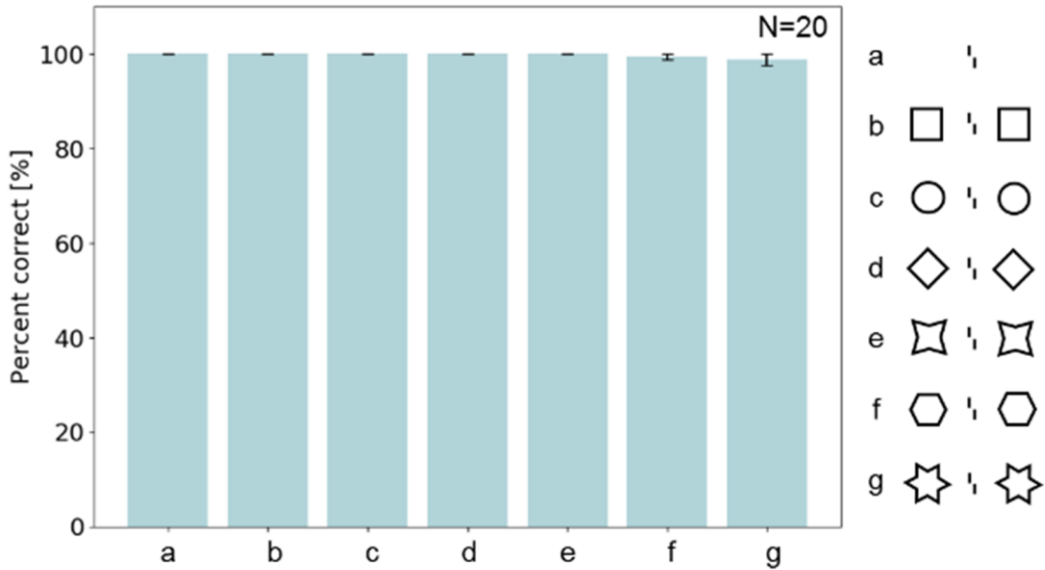
685 Plotting conventions are the same as in figure 2. Main hyperparameters are summarized at the bottom.

686

687 *Performance deterioration is due to crowding*

688 As a control to check that performance dropped because of crowding and not merely because of the  
 689 simultaneous presentation of a vernier target and another shape, we measured performance when  
 690 the vernier was presented outside, rather than inside, flanking shapes. Performance does not drop in

691 this case, compared to when the vernier is presented alone. This suggests that performance drops  
692 because of crowding in the networks.



693  
694 **Supplementary Figure 4: Performance deterioration is due to crowding.** The x-axis shows different conditions shown on  
695 the right, the y-axis shows vernier offset discrimination percent correct. Vernier accuracy does not decrease when the  
696 vernier is presented outside flanking shapes compared to the vernier alone condition.

697

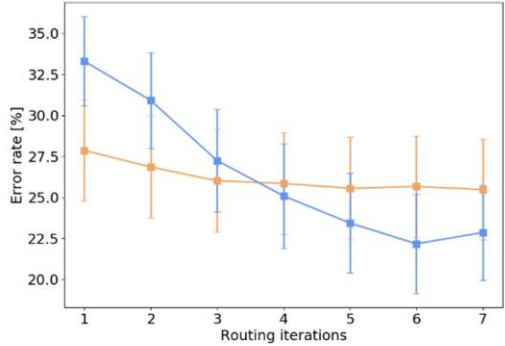
## 698 Experiment 2

699 *Results are robust against stimuli and hyperparameters changes*

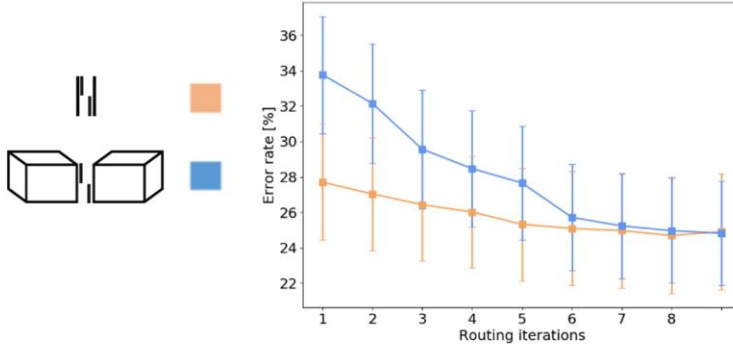
700 To avoid cherrypicking our hyperparameters, we ran several networks with different hyperparameter  
701 sets, and show that our results are robust with respect to these changes.

702 The results of experiment 2 remain qualitatively similar for different network hyperparameters. Below  
703 is a selection of results using different sets of hyperparameters. In both these cases, performance on  
704 the cuboids condition, but not the lines condition, drastically improves with the number of recurrent  
705 routing by agreement iterations (network a: lines:  $p = 0.041$  vs. cuboids  $p = 0.0005$ , network b: lines:  
706 0.11 vs. cuboids  $p=0.006$ ). In network a, the lines show a marginally significant improvement, but the  
707  $p$ -value is 100 times smaller than for the cuboids.

Model a. (N=36)



Model b. (N=32)



| Model                       | a            | b            |
|-----------------------------|--------------|--------------|
| Primary capsule types       | 4            | 4            |
| Primary capsule dims        | 1            | 1            |
| Secondary capsule types     | 4            | 4            |
| Secondary capsule dims      | 4            | 3            |
| Training routing iterations | 7            | 9            |
| Training steps              | 4000         | 4500         |
| Gaussian training noise     | [0.00, 0.02] | [0.00, 0.02] |
| Gaussian testing noise      | [0.00, 0.05] | [0.00, 0.05] |

708

709 **Supplementary Figure 5: Experiment 2 results are reproduced with different network hyperparameters.** The x-axis shows  
710 different numbers of routing iterations during testing and the y-axis shows the corresponding error rates (i.e., lower values  
711 indicate better performance). Error bars indicate standard deviation across N trained networks (see Methods).  
712 Performance increases drastically with recurrent routing iterations only for the cuboids condition, and not for the lines  
713 condition. A difference with the results shown in figure 3 is that performance with cuboids flankers is worse than  
714 performance with line flankers at early iterations. This may be explained by the far greater amount of pixels in cuboids  
715 than lines, increasing the interference between the cuboids and the vernier until the cuboids are segmented away. As the  
716 results exhibited in Figure 3 show, this effect can be mitigated through adequate hyperparameter choice. However, in this  
717 experiment, we focused on demonstrating that only the cuboids benefit from additional routing iterations, and this result  
718 is very stable across hyperparameter changes.